Formation of CuPd and CuPt Bimetallic Nanotubes by Galvanic Replacement Reaction

ARTICLE *in* THE JOURNAL OF PHYSICAL CHEMISTRY C · APRIL 2011

Impact Factor: 4.77 · DOI: 10.1021/jp112128g

THE JOURNAL OF PHYSICAL CHEMISTRY C

ARTICLE

pubs.acs.org/JPCC

Formation of CuPd and CuPt Bimetallic Nanotubes by Galvanic Replacement Reaction

Melinda Mohl,[†] Dorina Dobo,[†] Akos Kukovecz,[†] Zoltan Konya,[†,*] Krisztian Kordas,[‡,§] Jinquan Wei,[⊥] Robert Vajtai,[⊥] and Pulickel M. Ajayan[⊥]

[†]Department of Applied and Environmental Chemistry, University of Szeged, Rerrich B. tér 1., 6720 Szeged, Hungary

[‡]Microelectronics and Materials Physics Laboratories, University of Oulu, PL 4500 FIN-90014 Oulu, Finland

[§]Department of Chemistry, Technical Chemistry, Chemical-Biological Center, Umeå University, SE-90187 Umeå, Sweden

[⊥]Department of Mechanical Engineering and Materials Science, Rice University, Houston, Texas 77005, United States

Supporting Information

ABSTRACT: A galvanic replacement reaction has been successfully applied to prepare CuPd and CuPt bimetallic nanotubes. The nanotubes were characterized by transmission electron microscopy (TEM), scanning electron microscopy (SEM) combined with energy dispersive X-ray spectroscopy (EDS), and X-ray diffraction (XRD) techniques. Ultralong, single crystalline copper nanowires (NWs) with a diameter of ~64 nm and a length of several micrometers were used as template material. By controlling the amount of noble metal salt added, nanotubes with different compositions were obtained. After the replacement of Cu with Pt, nanotubes composed of a PtCu alloy were formed. EDS analysis revealed that the Pt content increased until about 66%. No further increase in the molar ratio resulted in any additional Pt incorporation into the alloy. As for the replacement of Cu with Pd, the thickening of the nanotubes was observed indicating that nanotubes composed of Pd nanoparticles were formed. Backscattered electron imaging and SEM-EDS revealed CuPd nanotubes with approximately 2.3% Cu content. These remarks indicate different evolution mechanism for the nanotubes in the two systems.

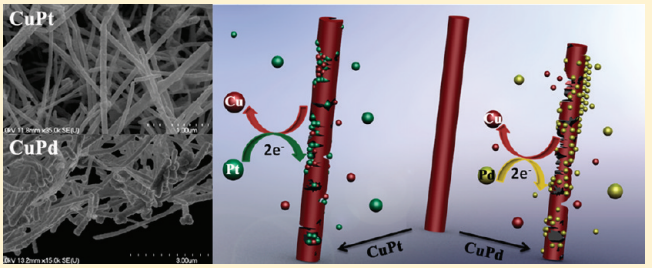

INTRODUCTION

Recently, research has been more and more preferably focused on the elaboration of the adjustability of shape, size, and surface properties of the colloidal nanostructures in the course of preparation. Relatively uniform hollow nanostructures can be prepared based on well controlled template nanostructures.[1,2] Thanks to their modifiable optical properties,[3] increased surface and low density, nanostructures with hollow textures have received outstanding attention in the last decades. Because their properties are different from those of the solid structures, they provide new possibilities for developing novel materials in application fields such as biomedical imaging,[4] optical sensors,[5] catalysis,[6,7] supported drug agents,[8] photothermal therapy,[9] and as building elements applicable in the field of ultralight structure materials.[10−12]

Unlike monometallic nanostructures, bimetallic ones exhibit properties that make the formation of new applications possible within one single nanostructure. To demonstrate this possibility, reference is made to the alloy brought about by combining gold and silver in nanostructures leading to favorable optical and catalytic properties at the same time.[13−15]

The outstanding properties in catalytic processes, stability at high temperatures, and resistance against both physical and chemical impacts make the platinum group metals quite distinguishable from other transition metals. The literature abounds in applications of Pt and Pd metals in the field of catalysis,[6] hydrogen storage,[16−18] and detecting hydrogen.[19] Because of their high activity toward oxygen reduction reactions (ORR), Pt-based electrocatalysts are very popular in proton-exchange membrane fuel cells (PEMFCs).[20] New catalysts with low cost and high ORR activity are continuously in great demand today. Recently, considerable interest has been devoted to Pd-bimetallic nanostructures exhibiting enhanced ORR activity compared to monometallic Pd electrocatalyst.[21−23] At the same time, Chen et al. demonstrated a new generation of supportless electrocatalysts based on Pt nanotubes (NTs) and PtPd NTs, which have the potential to combine the advantages of platinum-black and Pt/C catalysts while overcoming their drawbacks.[24]

When considering the potential preparation methods, the galvanic metal exchange reaction appears to be the most plausible and diverse way for producing bimetallic nanostructures[25−27] as it is well demonstrated by Xia and co-workers who exposed Ag nanostructures to solutions of Pt, Pd, and Au salts to prepare bimetallic hollow nanostructures.[28] This simple process has been

Received: December 21, 2010
Revised: April 5, 2011
Published: April 21, 2011

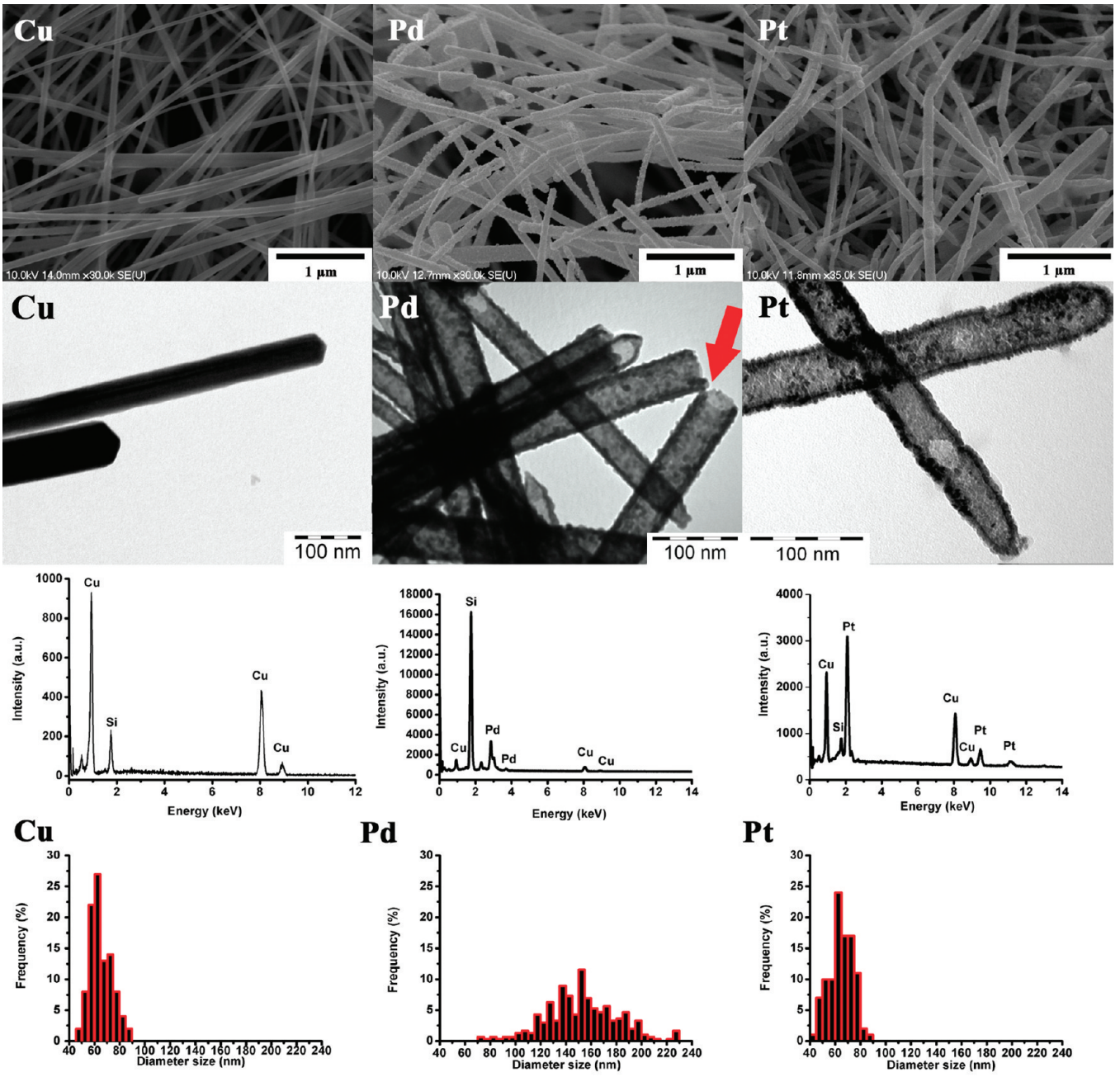

Figure 1. SEM and EDS and diameter size distribution of Cu NWs and CuPd NTs, CuPt NTs at molar ratio (K_2PtCl_4, K_2PdCl_4 to Cu) of 1.0 and TEM images of Cu NWs and CuPd NTs, CuPt NTs at molar ratio (K_2PtCl_4, K_2PdCl_4 to Cu) of 0.25.

also used to prepare porous noble metal nanostructures applying nanostructures of various transition metals (Ni, Co, Fe)[29−35] as sacrificial template. In a previous article, we have reported a protocol for synthesizing porous gold, platinum, and palladium nanorods via galvanic exchange reaction using Ni nanostructures as a sacrificial template.[36]

In this article, we describe a general approach to produce metallic nanotubes (NTs) by reacting noble metal solutions (Pt and Pd salts) with copper nanowires in organic media. Ultralong copper nanowires were synthesized in large-scale by a simple hydrothermal method.[37] Porous nanotubes of CuPt and CuPd were produced by exposing the Cu nanowires to K_2PtCl_4 and K_2PdCl_4 solutions, respectively.

EXPERIMENTAL SECTION

Chemicals. Reagent-grade chemicals such as potassium tetrachloro-palladate (K_2PdCl_4(II), Fluka), potassium tetrachloroplatinate (K_2PtCl_4(II), Aldrich), dimethyl-sulfoxid (C_2H_6OS, Molar), ethanol abs. (C_2H_6O, Molar chemical, 99,99%) were used as received without further purification.

(1). Synthesis of Cu NWs. Cu NWs were prepared by the method elaborated earlier.[37] After finishing the hydrothermal synthesis the NWs were centrifuged and washed with water, hexane, and ethanol. The ethanous suspension of NWs was dried in nitrogen atmosphere to protect the Cu NWs from oxidation. After the mass of NWs was measured, the sample was suspended

dx.doi.org/10.1021/jp112128g |J. Phys. Chem. C 2011, 115, 9403–9409

again and sonicated in a known amount of ethanol until a homogeneous suspension was achieved.

(2). Synthesis of Bimetallic CuPt, CuPd NTs. In a typical replacement reaction, 3 mL of copper nanowire suspension in ethanol (1 mg/mL) was sonicated for at least half an hour then centrifuged at 3200 rpm and washed with dimethyl sulfoxide (DMSO). The copper nanowires were then dispersed in DMSO and refluxed for 5 min in a 50 mL flask under nitrogen atmosphere. Aliquots of 1 mM noble metal salt in DMSO solution were added dropwise to the refluxing (~189 °C) solution and refluxed until its color became stable (typically 10 min). Vigorous stirring (~300 rpm) was maintained throughout all syntheses. A similar procedure was applied to form CuPd and CuPt nanotubes using potassium tetrachloro-palladate and potassium tetrachloro-platinate. Thereafter, the product was centrifuged and washed with water.

(3). Characterization. Product morphology and synthesis progress were assessed by transmission electron microscopy (TEM, Philips CM10). Samples were dropped on a copper mounted holey carbon film and dried. The statistical characterization of the diameter distribution of each sample was performed based on TEM and SEM images of 90k magnification.

The morphology and elemental composition of the prepared copper nanowires was characterized by scanning electron microscopy (Hitachi S-4700) and energy dispersive X-ray spectroscopy (EDS), respectively. Secondary electron SEM (SE-SEM) images were obtained by dropping samples on the surface of a piece of silicon wafer mounted on an aluminum sample holder. The accelerating voltage was set at 15 kV. For backscattering electron (BSE) images, samples were dropped on a copper mounted holey carbon film and dried.

For XRD analysis, a homogeneous suspension of the nanotubes was dropped on the surface of a glass slide heated at 40 °C and dried. The powder X-ray diffraction patterns were obtained using a Rigaku Miniflex II XRD instrument operating with Cu Kα radiation (λ = 1.5406 Å). The 2Θ Bragg angles were scanned over a range of 25−90° at a rate of 1.0° min^{-1}.

RESULTS AND DISCUSSION

Different amounts of 10^{-3} M K_2PdCl_4 or K_2PtCl_4 solutions were added to Cu NWs at the following molar ratios relative to the amount of Cu NWs: 0.10, 0.25, 0.50, 0.75, 1.00, and 1.50. Following the experiments, the samples were washed, centrifuged, and analyzed.

Mechanism. During the galvanic displacement reaction, the red color of the Cu nanowires suspension turned to dark gray indicating the formation of CuPt, CuPd nanotubes. Using Cu nanostructures as sacrificial templates instead of silver ones has two advantages: (i) lower cost and (ii) easier product purification, because the process is accompanied by the formation of $CuCl_2$, which is highly soluble in water and in polar solvents unlike the colloidal AgCl precipitates. As a reaction media DMSO, a polar aprotic solvent has been used because Cu NWs form agglomerates in distilled water. Several solvents such as ethanol, 2-propanol (Figure SI-1 of the Supporting Information), acetone, and so forth have been tested as reaction medium. Using either dimethyl sulfoxide or dimethyl formamid resulted in almost the same products. In the case of ethanol, both Pt and Pd ions are reduced leading to the formation of nanoparticles. The solubility of the metal salt and the boiling point of the solvent are of great significance. Compared to

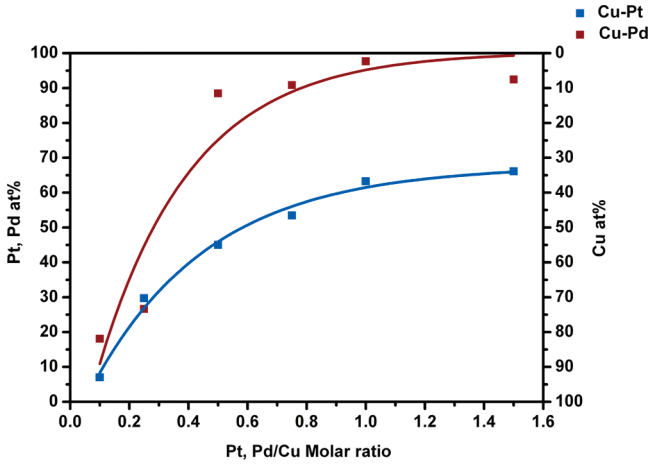

Figure 2. Atomic percentage of Cu and Pd, Pt in the product as a function of the molar ratio (K_2PtCl_4, K_2PdCl_4 to Cu) of the reactants.

DMSO, the acetone, izo-propanol, and ethanol have rather low boiling point. The crystallinity of the nanowires formed is influenced by the temperature to a great extent. In fact, in case of gold nanostructures at high temperature (100−200 °C) it has been observed that upon further refluxing the wall of the nanostructures underwent recrystallization.[25] Finally, DMSO proved to be the most eligible for this reaction because it is less toxic than the other polar aprotic solvents such as dimethylformamide (DMF).

The reaction takes place spontaneously because the standard reduction potentials of the $PtCl_4^{2-}$/Pt pair (0.74 V vs SHE) and the $PdCl_4^{2-}$/Pd pair (0.59 V vs SHE) are higher than the reduction potential of the Cu^{2+}/Cu pair (0.34 V vs SHE) and they can be reduced by Cu. Because of the standard reduction potential of $Cu^+ + e^- = 0.52$ V, the formation of Cu^{2+} is more favorable than that of Cu^+. The actual electrochemical reactions can be given as follows:

$$Cu(s) + PtCl_4^{2-}(aq) \rightarrow Pt(s) + Cu^{2+}(aq) + 4Cl^-(aq)$$
$$E = 0.395\ V$$

$$Cu(s) + PdCl_4^{2-}(aq) \rightarrow Pd(s) + Cu^{2+}(aq) + 4Cl^-(aq)$$
$$E = 0.25\ V$$

Figure 1 shows typical SEM and TEM images of the bimetallic nanotubes indicating that these structures inherited the wire shape of the initial nanowires. Compared to copper NWs the surface of these NTs is rougher. The diameter and length of the Cu NWs used as sacrificial template are about 64 ± 8 nm and several micrometers, respectively. The electron diffraction patterns[37] gave evidence for the Cu NWs to be single-crystalline in nature.

The CuPt and CuPd nanostructures shown in the TEM images (Figure 1) seem to be nearly transparent suggesting that they must have hollow interiors and, consequently, nanotubes must have been formed. The nanotube formation was observed by other groups[24,38] when reacting silver nanowires with noble metal salt solutions. Though the electron diffraction measurements indicated the presence of single-crystalline nanotubes (as it can be seen in Figure SI-2 of the Supporting Information), the TEM images clearly show nanotubes with grain boundaries. Supposedly, the single-crystalline particles (grains) take up an ordered form. Note that nanotubes were observed to undergo

dx.doi.org/10.1021/jp112128g |J. Phys. Chem. C 2011, 115, 9403–9409

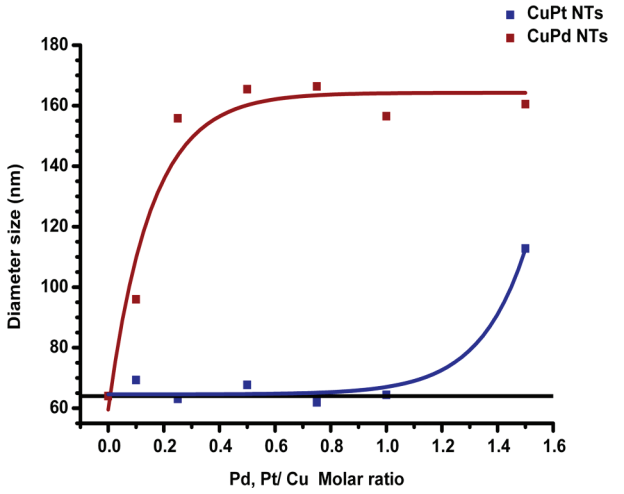

Figure 3. Diameter size of products as the function of the reactants molar ratio (K_2PtCl_4, K_2PdCl_4 to Cu).

aging and their structure disintegrated into smaller particles (Figure SI-2 of the Supporting Information) when stored under ambient conditions.

Quantification of Metal Content by EDS. Energy dispersive X-ray spectroscopy has been used to determine the composition of the nanotubes that were purified after the replacement reaction. The spectrum (Figure 1) displayed strong peaks for both Cu and Pt, Pd. The EDS analysis revealed a possible difference in the behavior of the CuPt and CuPd systems. Figure 2 shows the variation in noble metal and Cu atom % content of the nanotubes as a function of the molar ratio of the added noble metal (K_2PtCl_4, K_2PdCl_4) relative to the amount of copper. It is evident that the CuPd curve is much steeper. On the basis of these EDS results, at a molar ratio of about 1−1.5 the nanotubes are almost 100% composed of Pd, whereas in the corresponding CuPt system the Pt content is still below 70%.

Size Distribution. The variation of the nanotube diameter is shown in Figure 3. The diameter of the original sacrificial Cu NWs is 64 ± 8 nm (Figure 1). Electron microscopy analysis indicates that the extent of the diameter change is different for the two noble metal systems.

When exchanging copper with Pt, size increase was experienced only after the addition of more $PtCl_4^{2-}$ salt than the amount of Cu present. It is assumed that the addition of extra $PtCl_4^{2-}$ would lead to the deposition of platinum on the surface of the wires with the impact of increasing their diameter. It seems to be only possible in case of CuPd system that the Cu ions get rereduced from solution and get deposited on the surface of the nanotubes. Size increase was not observed in case of CuPt system contrary to CuPd system suggesting that probably the diffusion rate between the two metals is responsible for this phenomenon. This interdiffusion leads to the formation of CuPt alloy. This hypothesis is supported further by the fact that both the type (log-normal) and the variance of the nanotube diameter distribution curve measured at Cu/Pt = 1:1 molar ratio are very similar to those characteristic of the template Cu nanowires (Figure 1, bottom line). At a Cu/Pt molar ratio of 1:1, the average diameter of the nanotubes was found to be 64.4 nm with a standard deviation of 9.4 nm.

Contrary to this phenomenon, it is clearly seen that the size increase of the CuPd nanotubes has already been triggered by adding a small amount of $PdCl_4^{2-}$. At a molar ratio of 1:1 Cu NWs and $PdCl_4^{2-}$, the diameter of the nanotubes (152.7 ± 28.5 nm) was increased by more than 2.5 times. In this case it is supposed that the palladium content in $PdCl_4^{2-}$ is reduced and deposited on the surface of the nanowires rather than becoming part of the Cu crystal structure. This is confirmed by the evident deviation of the diameter size of the CuPd NTs of the Cu/Pd = 1:1 system to that of the original Cu NWs. Although the diameter distribution of the product NTs is a log-normal one, the variance is significantly larger than the corresponding Cu NW or CuPt NTs values indicating the possibility of diffusion controlled deposition process. In view of the above results, it is to be taken into account that the EDS results might be biased slightly by the thickening of the CuPd nanotubes.

XRD Analysis. The XRD analysis results are shown in Figure 4. The XRD records of nanotubes prepared by adding increasing amounts of $PdCl_4^{2-}$ to Cu NWs are presented in part A of Figure 4. Copper nanowires used as template material were identified on the basis of the three clearly distinguishable diffraction peaks at 2θ = 43.3°, 50.4°, and 74.2° corresponding to the {111}, {200}, and {220} crystal planes of face-centered cubic (fcc) copper, respectively. In some of the XRD records, the reflections of Cu_2O (JCPDS ICDD card 78−2076) appear at 2θ = 29.5°, 36.4°, 42.3°, 61.5°, and 73.6° corresponding to the {110}, {111}, {200}, {220}, and {311} crystal planes respectively of cubic copper(I) oxide. The appearance of Cu_2O can be attributed to the possible oxidation of Cu in the samples during storage and sample preparation. At a rather small (0.1) molar ratio Pd (JCPDS ICDD card 46−1043) peaks appear at 2θ = 39.8°, 46.6°, 67.2°, and 81.9° corresponding to the {111}, {200}, {220}, and {311} crystal planes respectively of face-centered cubic (fcc) palladium. Upon increasing the amount of K_2PdCl_4 added, the reflections characteristic for Cu and Cu_2O clearly disappear, although at a molar ratio of 1.0 a small peak indicating the presence of Cu_2O is still seen at 2θ = 29.5°. The presence of a small copper residue was also confirmed by EDS measurements up to 2.3% in the sample (part C of Figure 4).

Similar phenomena are shown in part B of Figure 4 for the CuPt system with Cu_2O reflections appearing in certain cases. Upon increasing the $PtCl_4^{2-}$ concentration, the Cu reflections are shifted toward smaller and smaller 2θ degree values and reflections of Cu_2O disappear. In part D of Figure 4 presenting the XRD records of NTs prepared at 1.0 molar ratio only reflections of CuPt alloy (JCPDS ICDD card *48−1549*) can be seen at 2θ = 41.0°, 47.7°, 69.7°, and 84.7° belonging to {111}, {200}, {220}, and {311} crystal planes, repectively. The EDS results are analogous with this because this sample contains at least 36.8% Cu according to the EDS measurement.

In Figure SI-3 of the Supporting Information, the *d* spacing calculated from the X-ray diffractograms is shown. The lattice constant of the NTs prepared at a molar ratio Pd to Cu of 1.0 was assessed to be 3.779 Å. This value is slightly smaller than that determined by JCPDS ICDD card 46−1043 (3.890 Å). The lattice constant of the Cu NTs applied as a template is 3.619 Å. The deviation might originate from a disordered crystal structure.

The lattice constant (3.753 Å) calculated for CuPt NTs is in good agreement with data found for CuPt alloy (3.796 Å) in the literature.

Tables SI-1 and SI-2 of the Supporting Information contain the peak positions of each sample of the CuPd and CuPt systems, respectively. Table SI-3 of the Supporting Information contains all of the JCPDS ICDD cards used to identify the composition of the nanotubes.

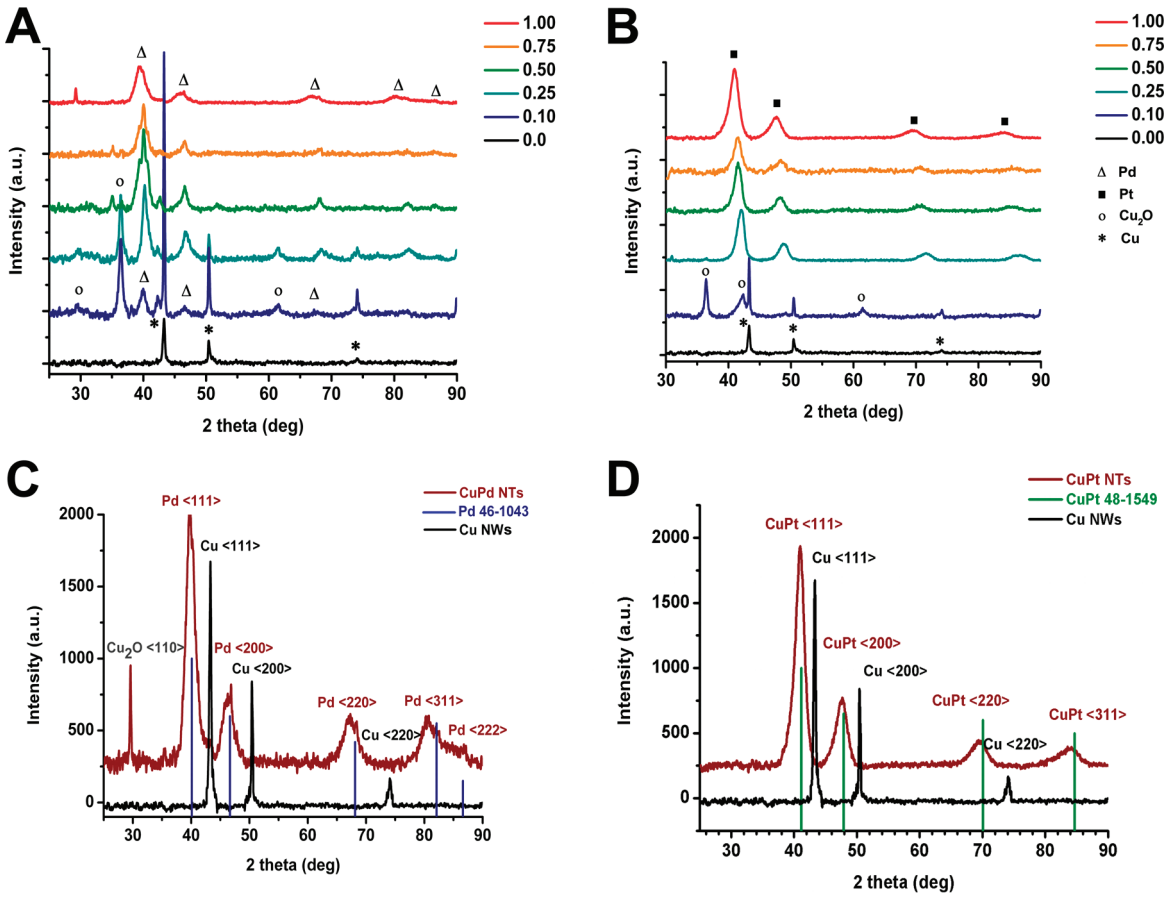

Figure 4. XRD patterns of the samples after exchanging the copper nanowires with (A) Pt and (B) Pd at different molar ratio of Cu and the noble metals. Panels (C) and (D) showing enlarged XRD patterns of the original Cu nanowires and the Pd as well as Pt exchanged products at a molar ratio (K_2PtCl_4, K_2PdCl_4 to Cu) of 1.0.

Formation Hypothesis. Small pits appearing (Figure 5) on the surface of the nanotubes suggest that the corrosion process must have been locally initiated rather than all over the surface. Dissolved Cl^- ions (coming from K_2PdCl_4, or K_2PtCl_4) play a significant role in the corrosion process of bulk metals and will act similarly for nanostructures. The adsorption of Cl^- ions on the surface is likely to enhance the rate of surface diffusion and thus can speed up the pitting process.[39] By examining the BSE images (Figure 5), we find that etch pits developed on the surface of the nanotubes indicating that oxidation removed Cu from the interior of the nanowires.

In the case of Pd, at about the K_2PdCl_4 to Cu molar ratio of 1:1 a Cu content of approximately 2.3% was determined by performing SEM-EDS analysis. It is assumed that the electrons of Cu atoms protruding through the holes formed on the surface are likely to reduce the $PdCl_4^{2-}$ ions in solution to form first palladium deposits and then a complete palladium coating preventing corrosion on the surface of the nanowires.[40,41] As further oxidation proceeded more and more, Pd NPs deposited and aggregated on the surface that resulted in a nanotube with rough and thick walls. Because the EDS analysis confirmed only 2.3% of Cu content, it is assumed that the nanostructures have hollow interiors (Figure 1, TEM image of CuPd NTs) even though they appear closed at the tips on the SEM image (Figure 1, SEM image of CuPd NTs). Upon increasing the molar ratio, the diameter of the nanotubes increases. Although EDS indicates that upon increasing the molar ratio the Cu content is significantly reduced, attention should be paid to the fact that due to the thickening of the wall the measured Cu content could be biased and smaller than the real value. The XRD analysis shows no formation of CuPd alloy suggesting that at this temperature and in this solution CuPd alloy is not likely to be formed. The nucleation and growth of Pd nanoparticles on the surface of the nanotubes leads to the thickening of the nanotubes.

As for Pt, the XRD analysis suggests that Pt probably diffuses into the copper to form a homogeneous alloy. Upon adding more and more K_2PtCl_4 solution to the system, the Pt content increased until about 66%. No further increase in the molar ratio resulted in any additional Pt incorporation into the alloy. This apparent threshold in the galvanic replacement reaction is probably due to reaching a critical point in the process of rapidly forming a homogeneous alloy as a result of the electrochemical impacts raised by the potential difference of the two metals. It is assumed that in the early stage $PtCl_4^{2-}$ reacts with pure copper, whereas as the reaction proceeds the reaction surface changes to a less reactive CuPt surface. This reaction resulted in the product CuPt alloy structures. Figure 6 shows a schematic image of the possible formation of CuPd bimetallic NTs and CuPt alloyed NTs.

We attribute the difference in the behavior of the two systems to Kirkendall mass-transport phenomena.[29] Kirkendall was the first to report an experimental proof that atomic diffusion occurs

dx.doi.org/10.1021/jp112128g |J. Phys. Chem. C 2011, 115, 9403–9409

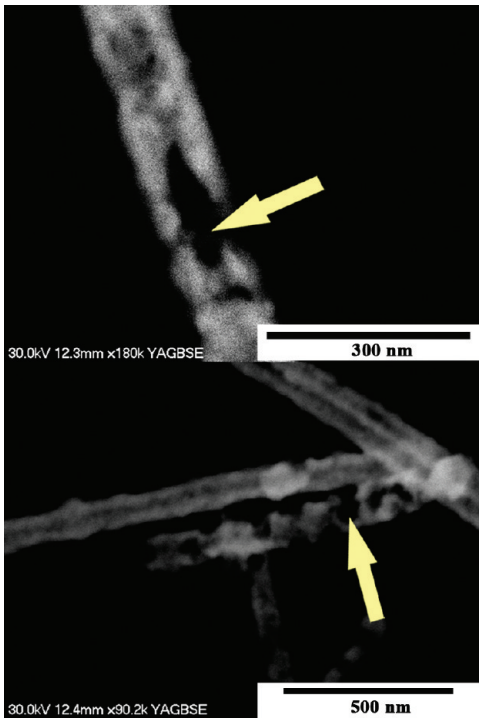

Figure 5. BSE images of CuPd NTs and CuPt NTs at a molar ratio (K_2PtCl_4, K_2PdCl_4 to Cu) of 1.5.

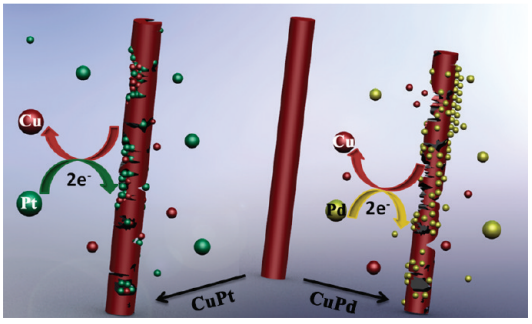

Figure 6. Schematic image illustrating the possible formation mechanism of CuPt alloy nanostructures (left) and CuPd bimetallic nanotubes (right) from Cu nanowires (middle). Green, yellow, and red spheres represent $Pd/PdCl_4^{2-}$, $Pt/PtCl_4^{2-}$, and Cu^{2+} ions.

through vacancies. McIlwarth et al. observed some differences in the structures of Cu@Pt and Pt@Cu core−shell nanostructures, which are attributed to different diffusion rates because the diffusion of Pt into Cu is fast relative to Cu diffusion into Pt.[42] Bélanger et al. demonstrated a detailed study of the electroless deposition of Pd on Cu metal islands deposited on graphite electrode.[43] They have found that the resulting morphology is highly dependent on the $PdCl_2$ amount used. For a concentration below 5 mM $PdCl_2$, Pd atoms partially covered the Cu surface hence Cu atoms covered by Pd as well as bare Cu atoms are oxidized and dissolved from the surface. This phenomenon involves the formation of a Pd shell on a Cu core. At higher $PdCl_2$ concentrations, a Pd shell enclosing a core of copper is formed. In fact, the CuPd system is a well-known binary alloy, however, at room temperature the alloy formation is rather hindered due to the low interdiffusion velocities. It is the difference in the electrochemical potentials occurring in the course of the reaction that can be held responsible for the morphological differences appearing at higher temperatures. The CuPt alloy formed in the case of the Pt exchange can have a higher electrochemical potential that blocks the oxidation of Cu. On adding a bigger amount of Pt salt, the excess Cu and Pt ions in solution can be further reduced and deposited on the surface leading to thickening. Because no alloy is formed in the course of the Pd exchange, the difference in the electrochemical potential allows for the oxidation of almost the whole Cu NW and the deposition of Pd on the surface.

Electrocatalyst durability pose severe challenge for scientists that must be addressed before the commercialization of PEMFCs.[24] Supported Pt-based materials, such as Pt/C catalyst, are probably the most frequently used cathode catalysts owing to their high catalytic activity toward oxygen reduction reaction. Lately, alternative nonplatinum catalysts received outstanding attention because of low cost, enhanced durability, and high ORR activity. Recently several groups demonstrated that Pd nanostructures combined with certain transition metals exhibit enhanced catalytic activity toward ORR.[22,23,34,44] Ding et al. described the fabrication of novel CuPd bimetallic nanocomposites with nanotubular mesoporous morphology through a simple galvanic replacement reaction. Surprisingly, significantly higher ORR activity was observed on the resulted CuPd nanostructure compared to the commercially available Pt/C catalyst.[34] Previously, Ding et al. have successfully fabricated CuPt bimetallic nanostructures that showed high activity toward methanol electrooxidation with enhanced CO tolerance.[45] As described elsewhere,[46,47] the CuPd system has also been successfully applied in the electrocatalytic reduction of the nitrate.

In this report, we described a simple approach to synthesizing potentially useful CuPd and CuPt bimetallic nanotubes by the galvanic replacement reaction of Cu nanowires. Both CuPd and CuPt bimetallic nanotubes may find application in catalytic and sensing applications where a high surface to volume ratio is required.

CONCLUSIONS

In conclusion, Cu NWs dispersed in DMSO can be transformed into CuPt and CuPd nanotubes by reacting them with either K_2PtCl_4 or K_2PdCl_4. By controlling the molar ratio of K_2PtCl_4 or K_2PdCl_4 to Cu, nanotubes of different composition can be synthesized. Replacement of Cu with Pt will result in the formation of CuPt alloy nanotubes. Nanotubes formed by the replacement of Cu with Pd were instead composed of CuPd at a low Pd/Cu molar ratio and almost pure Pd at a high Pd/Cu ratio. The synthesis reactions could be fully interpreted based on available electrochemical data and the Kirkendall effect. The reported procedure presents a facile new method for tailoring the properties of ultralong noble metal nanotubes.

ASSOCIATED CONTENT

Supporting Information. SEM images of products of the CuPt exchange reaction in ethanol and in DMF (Figure SI-1) and electron diffraction patterns (Figure SI-2) of CuPt nanotubes and CuPd nanotubes. CuPt and CuPd nanostructures' aging was observed that are shown on TEM images (Figure SI-3). The *d* spacing of CuPd NWs and CuPt NWs at a molar ratio (K_2PtCl_4, K_2PdCl_4 to Cu) of 1.0 (Figure S-4). Tables of comparaison

(Tables SI-1−SI-3) of XRD reflexions. This material is available free of charge via the Internet at http://pubs.acs.org.

AUTHOR INFORMATION

Corresponding Author

*E-mail: konya@chem.u-szeged.hu, Tel: +36-62-544-620, Fax: +36-62-544-619.

ACKNOWLEDGMENT

The financial support of the Hungarian Scientific Research Fund (OTKA) through projects NNF2-85889 and 73676 is acknowledged.

REFERENCES

(1) Jin, R.; Charles, C., Y.; Hao, E.; Metraux, G. S.; Schatz, G. C.; Mirkin, C. A. *Nature* **2003**, *425*, 487–490.
(2) Peng, X.; Manna, L.; Yang, W.; Wickham, J.; Scher, E.; Kadavanich, A.; Alivisatos, A. P. *Nature* **2000**, *404*, 59–61.
(3) Au, L.; Chen, Y.; Zhou, F.; Camargo, P. H. C.; Lim, B.; Li, Z. Y.; Ginger, D. S.; Xia, Y. *Nano Res.* **2008**, *1*, 441–449.
(4) Chen, J.; Wiley, B.; Li, Z. Y.; Campbell, D.; Saeki, F.; Cang, H.; Au, L.; Lee, J.; Li, X.; Xia, Y. *Adv. Mater.* **2005**, *17*, 2255–2261.
(5) Sun, Y.; Xia, Y. *Anal. Chem.* **2002**, *74*, 5297–5305.
(6) Kim, S.-W.; Kim, M.; Lee, W. Y.; Hyeon, T. *J. Am. Chem. Soc.* **2002**, *124*, 7642–7643.
(7) Liu, Z.; Hong, L.; Tham, M. P.; Lim, T. H.; Jiang, H. *J. Power Sources* **2006**, *161*, 831–835.
(8) Portney, N.; Ozkan, M. *Anal. Bioanal. Chem.* **2006**, *384*, 620–630.
(9) Au, L.; Zheng, D.; Zhou, F.; Li, Z.-Y.; Li, X.; Xia, Y. *ACS Nano* **2008**, *2*, 1645–1652.
(10) Schwarz, U. S.; Safran, S. A. *Phys. Rev. E: Stat.* **2000**, *62*, 6957.
(11) Sanders, W. S.; Gibson, L. J. *Mater. Sci. Eng., A* **2003**, *352*, 150–161.
(12) Caruso, F.; Caruso, R. A.; Möhwald, H. *Science* **1998**, *282*, 1111–1114.
(13) Cao, L.; Tong, L.; Diao, P.; Zhu, T.; Liu, Z. *Chem. Mater.* **2004**, *16*, 3239–3245.
(14) Zhang, J.; Lima, F. H. B.; Shao, M. H.; Sasaki, K.; Wang, J. X.; Hanson, J.; Adzic, R. R. *J. Phys. Chem. B* **2005**, *109*, 22701–22704.
(15) Damle, C.; Biswas, K.; Sastry, M. *Langmuir* **2001**, *17*, 7156–7159.
(16) Dresselhaus, M. S.; Thomas, I. L. *Nature* **2001**, *414*, 332–337.
(17) Schlapbach, L.; Zuttel, A. *Nature* **2001**, *414*, 353–358.
(18) Ward, M. D. *Science* **2003**, *300*, 1104–1105.
(19) Lauhon, L. J.; Gudiksen, M. S.; Wang, D.; Lieber, C. M. *Nature* **2002**, *420*, 57–61.
(20) Markovic, N. M.; Ross, P. N. *Electrochim. Acta* **2000**, *45*, 4101–4115.
(21) Fernández, J. L.; Walsh, D. A.; Bard, A. J. *J. Am. Chem. Soc.* **2004**, *127*, 357–365.
(22) Wang, X.; Kariuki, N.; Vaughey, J. T.; Goodpaster, J.; Kumar, R.; Myers, D. J. *J. Electrochem. Soc.* **2008**, *155*, B602–B609.
(23) Shao, M.-H.; Sasaki, K.; Adzic, R. R. *J. Am. Chem. Soc.* **2006**, *128*, 3526–3527.
(24) Chen, Z.; Waje, M.; Li, W.; Yan, Y. *Angew. Chem., Int. Ed.* **2007**, *46*, 4060–4063.
(25) Sun, Y.; Mayers, B.; Xia, Y. *Adv. Mater.* **2003**, *15*, 641–646.
(26) Yang, J.; Lee, J. Y.; Too, H.-P. *J. Phys. Chem. B* **2005**, *109*, 19208–19212.
(27) Yin, Y.; Erdonmez, C.; Aloni, S.; Alivisatos, A. P. *J. Am. Chem. Soc.* **2006**, *128*, 12671–12673.
(28) Sun, Y.; Xia, Y. *Science* **2002**, *298*, 2176–2179.
(29) Yin, Y.; Rioux, R. M.; Erdonmez, C. K.; Hughes, S.; Somorjai, G. A.; Alivisatos, A. P. *Science* **2004**, *304*, 711–714.
(30) Vasquez, Y.; Sra, A. K.; Schaak, R. E. *J. Am. Chem. Soc.* **2005**, *127*, 12504–12505.
(31) Chou, N. H.; Schaak, R. E. *J. Am. Chem. Soc.* **2007**, *129*, 7339–7345.
(32) Chen, C.; Loo, J.; Deng, M.; Kox, R.; Huys, R.; Bartic, C.; Maes, G.; Borghs, G. *J. Phys. Chem. C* **2009**, *113*, 5472–5477.
(33) Zhang, J.; Qiu, C.; Ma, H.; Liu, X. *J. Phys. Chem. C* **2008**, *112*, 13970–13975.
(34) Xu, C.; Zhang, Y.; Wang, L.; Xu, L.; Bian, X.; Ma, H.; Ding, Y. *Chem. Mater.* **2009**, *21*, 3110–3116.
(35) Liang, H. P.; Zhang, H. M.; Hu, J. S.; Guo, Y. G.; Wan, L. J.; Bai, C. L. *Angew. Chem., Int. Ed.* **2004**, *43*, 1540–1543.
(36) Mohl, M.; Kumar, A.; Reddy, A. L. M.; Kukovecz, A.; Konya, Z.; Kiricsi, I.; Vajtai, R.; Ajayan, P. M. *J. Phys. Chem. C* **2009**, *114*, 389–393.
(37) Mohl, M.; Pusztai, P.; Kukovecz, A.; Konya, Z.; Kukkola, J.; Kordas, K.; Vajtai, R.; Ajayan, P. M. *Langmuir* **2010**, *26*, 16496–16502.
(38) Bi, Y.; Lu, G. *Chem. Mater.* **2008**, *20*, 1224–1226.
(39) Newman, R. C.; Sieradzki, K. *Science* **1994**, *263*, 1708–1709.
(40) Xiong, Y.; Wiley, B.; Chen, J.; Li, Z.-Y.; Yin, Y.; Xia, Y. *Angew. Chem., Int. Ed.* **2005**, *44*, 7913–7917.
(41) Xiong, Y.; Chen, J.; Wiley, B.; Xia, Y.; Aloni, S.; Yin, Y. *J. Am. Chem. Soc.* **2005**, *127*, 7332–7333.
(42) Zhou, S.; Varughese, B.; Eichhorn, B.; Jackson, G.; McIlwrath, K. *Angew. Chem., Int. Ed.* **2005**, *44*, 4539–4543.
(43) Ghodbane, O.; Roué, L.; Bélanger, D. *Chem. Mater.* **2008**, *20*, 3495–3504.
(44) Sarkar, A.; Murugan, A. V.; Manthiram, A. *J. Phys. Chem. C* **2008**, *112*, 12037–12043.
(45) Xu, C.; Wang, L.; Wang, R.; Wang, K.; Zhang, Y.; Tian, F.; Ding, Y. *Adv. Mater.* **2009**, *21*, 2165–2169.
(46) de Vooys, A. C. A.; van Santen, R. A.; van Veen, J. A. R. *J. Mol. Catal. A: Chem.* **2000**, *154*, 203–215.
(47) Matatov-Meytal, U.; Sheintuch, M. *Catal. Today* **2005**, *102−103*, 121–127.